

RESEARCH ARTICLE

Inhibition of cargo export at ER exit sites and the trans-Golgi network by the secretion inhibitor FLI-06

Yoji Yonemura¹, Xiaolin Li¹, Katja Müller¹, Andreas Krämer¹, Paul Atigbire¹, Torben Mentrup¹, Talitha Feuerhake¹, Torsten Kroll¹, Olga Shomron², Richard Nohl³, Hans-Dieter Arndt³, Christian Hoischen¹, Peter Hemmerich¹, Koret Hirschberg^{2,*} and Christoph Kaether^{1,*}

ABSTRACT

Export out of the endoplasmic reticulum (ER) involves the Sar1 and COPII machinery acting at ER exit sites (ERES). Whether and how cargo proteins are recruited upstream of Sar1 and COPII is unclear. Two models are conceivable, a recruitment model where cargo is actively transported through a transport factor and handed over to the Sar1 and COPII machinery in ERES, and a capture model, where cargo freely diffuses into ERES where it is captured by the Sar1 and COPII machinery. Using the novel secretion inhibitor FLI-06, we show that recruitment of the cargo VSVG to ERES is an active process upstream of Sar1 and COPII. Applying FLI-06 before concentration of VSVG in ERES completely abolishes its recruitment. In contrast, applying FLI-06 after VSVG concentration in ERES does not lead to dispersal of the concentrated VSVG, arguing that it inhibits recruitment to ERES as opposed to capture in ERES. FLI-06 also inhibits export out of the trans-Golgi network (TGN), suggesting that similar mechanisms might orchestrate cargo selection and concentration at the ER and TGN. FLI-06 does not inhibit autophagosome biogenesis and the ER-peroxisomal transport route, suggesting that these rely on different mechanisms.

KEY WORDS: VSVG, ER exit sites, ER export, COP II, Secretory pathway, Secretion, Trans-Golgi network

INTRODUCTION

The secretory pathway comprises the endoplasmic reticulum (ER), the ER exit sites (ERES), the ER-Golgi intermediate compartment (ERGIC), the Golgi, the trans-Golgi network (TGN), post-Golgi vesicles and carriers between compartments. Transport between the organelles primarily involves sorting and concentration of cargo into specialized membrane domains. This is followed by budding of a transport carrier, sometimes involving a coat structure, transport of this carrier to the destination and fusion with the target membrane. Although in principle similar, transport steps at different organelles are mediated by different machineries. Export out of the ER, for example, is orchestrated by the COPII coat machinery (reviewed in Zanetti et al., 2011), whereas COPI coats are involved in intra-Golgi transport and

retrograde Golgi to ER transport (reviewed in Barlowe and Miller, 2013; Popoff et al., 2011). Exit from the TGN is mediated by clathrin (to endosomes) and by unknown coats (to the plasma membrane, Guo et al., 2014). Different transport steps involve different GTPases, for example Sar1 (in mammals there are two isoforms, SAR1A and SAR1B) in the ER exit and Arf1 in ER-Golgi transport and within the Golgi, as well as a distinct sets of Rab proteins and their GAPs and GEFs (reviewed in Barlowe and Miller, 2013; Pfeffer, 2013; Zanetti et al., 2011). According to current models for ER export, COPII assembly is initiated at ERES (Bannykh et al., 1996) by GDP-GTP exchange on Sar1 mediated by Sec12 (also known as PREB in mammals) (reviewed in Zanetti et al., 2011). Activated Sar1 induces membrane-curvature and recruits Sec23–Sec24 heterodimers (each of which have more than one isoform in mammals). Sec24 binds to export signals on transmembrane cargo proteins destined to be exported out of the ER directly or indirectly via adaptors. Finally the outer coat components Sec13 and Sec31 (SEC31A and SEC31B in mammals) are recruited and scission is initiated (reviewed in Venditti et al., 2014). *In vitro*, vesicle budding can be mediated by purified Sar1, Sec23–Sec24 and Sec13–Sec31 alone (Barlowe et al., 1994; Salama et al., 1993), but *in vivo* additional proteins and mechanisms might be involved. For selecting and concentrating large cargo proteins in the ER, specifically procollagens, additional ‘helpers’ like TANGO1 (also known as MIA3), cTAGE5 and sedlin have been described (Saito et al., 2009, 2011; Venditti et al., 2012). Procollagens are secreted proteins. In contrast to them, transmembrane proteins can directly bind through cytosolic transport signals to Sec24 (Miller et al., 2003; Wendeler et al., 2007), but additional factors like Erv14 (cornichon homolog 1) are important for export of at least some cargo (Bokel et al., 2006; Pagant et al., 2015). Little is known about the ER export of GPI-anchored proteins, but p24 family members seem to be involved (Castillon et al., 2009; Fujita et al., 2011; Schimmoller et al., 1995).

Are cargo proteins actively selected and recruited to ERES, or alternatively do they freely diffuse into ERES and get captured and subsequently concentrated by binding to Sec24? Are there common mechanisms of cargo selection and concentration at different transport steps along the secretory pathway?

To address these questions we here made use of a recently described secretion inhibitor, FLI-06, in HeLa cells (Krämer et al., 2013). This novel inhibitor acts differently from Brefeldin A (BFA) at an earlier transport step, before or at ERES. Using FLI-06 we were able to establish that cargo is actively recruited to ERES as opposed to freely diffusing into ERES and being captured there. We also show that common mechanisms must exist between export out of the ER and out of the TGN, but not other ER export routes to peroxisomes and autophagosomes.

¹Leibniz Institut für Altersforschung-Fritz Lipmann Institut, Jena 07745, Germany.

²Pathology Department, Sackler School of Medicine, Tel-Aviv University, Tel-Aviv 69978, Israel. ³Lehrstuhl für organische Chemie I, Friedrich-Schiller Universität, Jena 07743, Germany.

*Authors for correspondence (koty@post.tau.ac.il; ckaether@fli-leibniz.de)

© P.A., 0000-0001-9032-4583; C.K., 0000-0002-6874-2276

RESULTS

FLI-06 does not affect folding of secreted proteins

The novel secretion inhibitor FLI-06 (Krämer et al., 2013) blocks accumulation of cargo in ERES resulting in a uniform ER-distribution of cargo, although ERES are still present. A simple explanation for this phenotype would be that FLI-06 inhibits general folding of nascent proteins in the ER and/or immobilizes them. To rule out these possibilities, we first tested whether FLI-06 affects the folding and mobility of VSVG–EYFP, a well characterized model transport protein (Toomre et al., 1999). VSVG throughout the text refers to VSVGtsO45, a temperature-sensitive mutant of the vesicular stomatitis virus G-protein, which misfolds at 40°C and cannot leave the ER (Gallione and Rose, 1985). Upon incubation at 32°C, the permissive temperature, VSVG folds correctly and leaves the ER through ERES (Presley et al., 1997; Scales et al., 1997). FLI-06 does not inhibit the correct, export-competent folding of VSVG, as demonstrated by the immunostaining with a folding-specific anti-VSVG-antibody (Fig. 1A). It also does not inhibit VSVG trimer formation, a further prerequisite for ER export (Kreis and Lodish, 1986), as demonstrated by western blotting in non-reducing conditions (Fig. 1B). Next, we tested whether FLI-06 inhibits cargo recruitment due to changes in diffusion in the ER membrane. To this end, we determined the lateral diffusion of VSVG–EYFP in fluorescence recovery after photobleaching (FRAP) experiments at 40°C (Fig. 1C,D). To ensure even distribution of membranes in the bleached area, we depolymerized microtubules with nocodazole, which is known to induce ER sheets. VSVG–EYFP in the ER membrane recovered with a $t_{1/2}$ of 9.5 s into the bleached area, which is within range of published results (Dukhovny et al., 2008; Nehls et al., 2000). Interestingly, in the presence of 10 μ M FLI-06, recovery rates were faster (7.5 ± 0.5 s versus 9.5 ± 0.5 s, mean \pm s.d.; Fig. 1C,D). Collectively, these data indicate that FLI-06 does not inhibit recruitment to ERES by interfering with protein folding or immobilizing cargo in the ER.

Secretory cargo is recruited to ERES, not captured in ERES

Recruitment of cargo to ERES is an ill-defined process. Two alternative models are conceivable, a ‘recruitment’ and a ‘capture’ model. In the recruitment model, cargo that is destined to be exported out of the ER must be actively recruited and transported into ERES. In the capture model, potential cargo freely diffuses into and out of ERES and is concentrated there by binding directly or indirectly to Sar1 and Sec23–Sec24. The FLI-06 phenotype, diffuse distribution of cargo in the ER, can be explained by an inhibition of recruitment of cargo into ERES, but also by blocking the capture of cargo in ERES. To get more insights into the mechanisms of FLI-06, we tested whether it would inhibit recruitment of cargo to ERES or inhibit a capture mechanism in ERES. To this end we induced giant ERES (gERES) by treating VSVG–EYFP-transfected cells with Brefeldin A (BFA) and nocodazole (Dukhovny et al., 2008). In this regimen, export cargo, VSVG–EYFP in this case, is recruited into gERES, but further export out of ERES is blocked. HeLa cells were transfected with VSVG–EYFP, incubated at 40°C overnight, and gERES were induced with BFA and nocodazole at 32°C (Fig. 2A). FLI-06 was either added directly at the 32°C shift, before VSVG–EYFP concentrated in gERES (Fig. 2A, BNF), or after 45 min at 32°C, after VSVG–EYFP concentration in gERES (Fig. 2A, BN+F). The total incubation time at 32°C was 135 min. DMSO was added as control (Fig. 2A, BN). To quantify concentration in gERES, the variance in pixel intensity (PFIvar) was used as described in Dukhovny et al. (2008). As shown before (Dukhovny et al., 2008), addition of BFA and nocodazole at 32°C

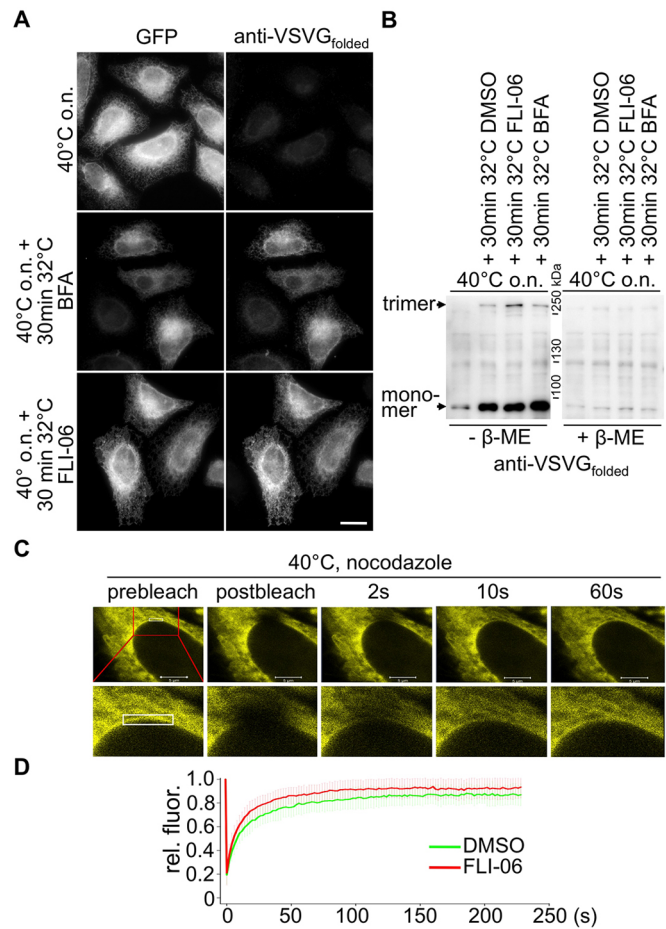


Fig. 1. FLI-06 does not inhibit folding or mobility of proteins in the ER. HeLa cells transiently transfected with VSVG–EYFP were incubated overnight (o.n.) at 40°C to accumulate VSVG–EYFP in the ER or were additionally incubated with 1 μ g/ml BFA or 10 μ M FLI-06 for 30 min at 32°C. Cells were then fixed and processed for immunofluorescence with folding-specific anti-VSVG antibodies (A) or lysed, separated by SDS-PAGE and probed for folding-specific anti-VSVG antibodies (B). Scale bar: 10 μ m. Images in A were acquired and processed with identical settings. $\pm\beta$ -ME, presence or absence of β -mercaptoethanol in the sample buffer. (C) FRAP analysis of VSVG–EYFP diffusion in the ER. HeLa cells transfected with VSVG–EYFP were treated with 1 μ g/ml nocodazole for 20 min at 40°C. The nuclear membrane of cells additionally treated with DMSO or FLI-06 (10 μ M) were photobleached and recovery rates determined as exemplified for a DMSO-treated cell. The bleached area (white box) is shown in the lower row at a higher magnification. Scale bar: 5 μ m. (D) VSVG–EYFP recovery dynamics. Mean VSVG–EYFP FRAP recovery curves for DMSO- (green) and FLI-06-treated HeLa cells (red). Data points show mean \pm s.d. ($n=31$ and 41 for untreated and treated cells, respectively, from three independent experiments).

resulted in the formation of many gERES after 45 min (Fig. 2A, top panel) and a threefold increase in PFIvar (Fig. 2B). Prolonged incubation resulted in a further increase in size and intensity of the gERES. In contrast, when FLI-06 was present throughout the 32°C chase, no gERES became visible (Fig. 2A, middle panel), and PFIvar only slightly increased (Fig. 2B), confirming that FLI-06 inhibits cargo accumulation in ERES (Krämer et al., 2013). When FLI-06 was added after formation of gERES, they remained stable, but a slow decline in number of gERES was observed over time, accompanied by an increase in ER labeling. This was also reflected by a decrease in PFIvar (Fig. 2A, lower panel, Fig. 2B). Accumulation of VSVG in ERES in cells treated

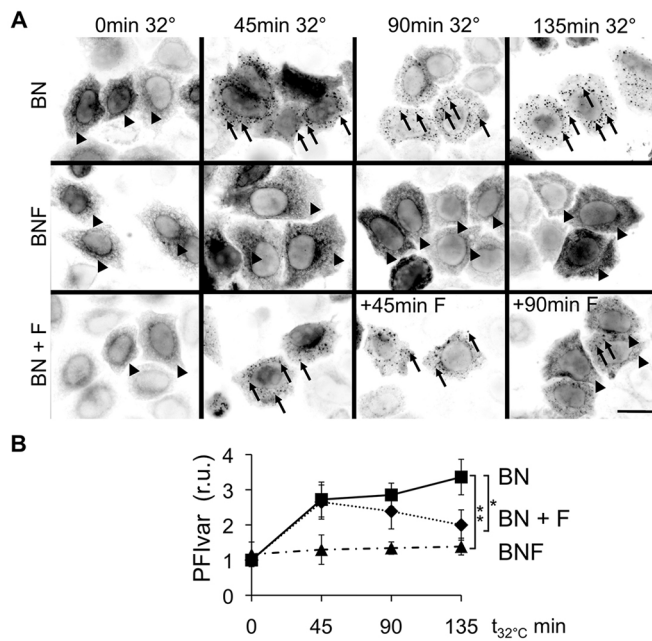


Fig. 2. Cargo is concentrated in ERES by a recruitment mechanism.

(A) HeLa cells transiently transfected with VSVG–EYFP were incubated overnight at 40°C to accumulate VSVG–EYFP in the ER. Cells were then incubated on ice for 30 min with 5 µg/ml BFA and 1 µg/ml nocodazole (denoted BN) and chased in this BFA- and nocodazole-containing medium for indicated times at 32°C. FLI-06 (10 µM) was added together with BFA and nocodazole (denoted BNF) or after 45 min at 32°C (denoted BN+F). DMSO served as control. Thereafter cells were fixed and imaged by fluorescence microscopy. Inverted images of representative cells from at least $n=3$ independent experiments are shown. Scale bar: 10 µm. Arrowheads, diffuse ER staining; arrows, giant (g) ERES. (B) Quantitation of A. Displayed is the relative variance in pixel fluorescence intensity (PFivar) in relative units (r.u.), where 1 is the mean value of cells after overnight incubation at 40°C. Displayed are the mean±s.d. of 80–100 regions of interest (ROIs) from three different experiments. * $P<0.05$, ** $P<0.01$ (one-way analysis of variance followed by Dunnett's multiple comparison test).

with BFA and nocodazole is known to undergo cycles of concentration and rapid collapse (Dukhovny et al., 2008). The slow decline of gERES number and PFivar can therefore be explained by a prevented re-entry of cargo into gERES after addition of FLI-06. The data are consistent with the cargo recruitment model, where FLI-06 inhibits the entry of cargo into ERES, not the capture of cargo in ERES. In the latter case a fast concomitant decline of intensity in all gERES would be expected after adding the compound. Further support for the recruitment model came from live-cell imaging of single gERES in the presence and absence of FLI-06. No decrease in average lifetime of single gERES was observed in FLI-06-treated cells (Fig. 3A; Movie 1). Rather, quantification showed an increase in average lifetime of gERES (Fig. 3B) and a strong reduction in the ratio of newly forming versus dissolving gERES in FLI-06-treated cells (Fig. 3C). This strong reduction was indeed due to a strong reduction in newly forming gERES, not to more dissolving gERES (Fig. 3D). Quantifying the intensity profile of single gERES over time showed the typical increase-collapse-increase profile in DMSO-treated cells as described in Dukhovny et al. (2008). In contrast, in FLI-06-treated cells, fluorescence intensity in gERES plateaued over several minutes. This was followed by collapse and no further entry of VSVG–EYFP into gERES, consistent with a block in recruitment (Fig. 3E). Taken together, FLI-06 inhibits the recruitment into

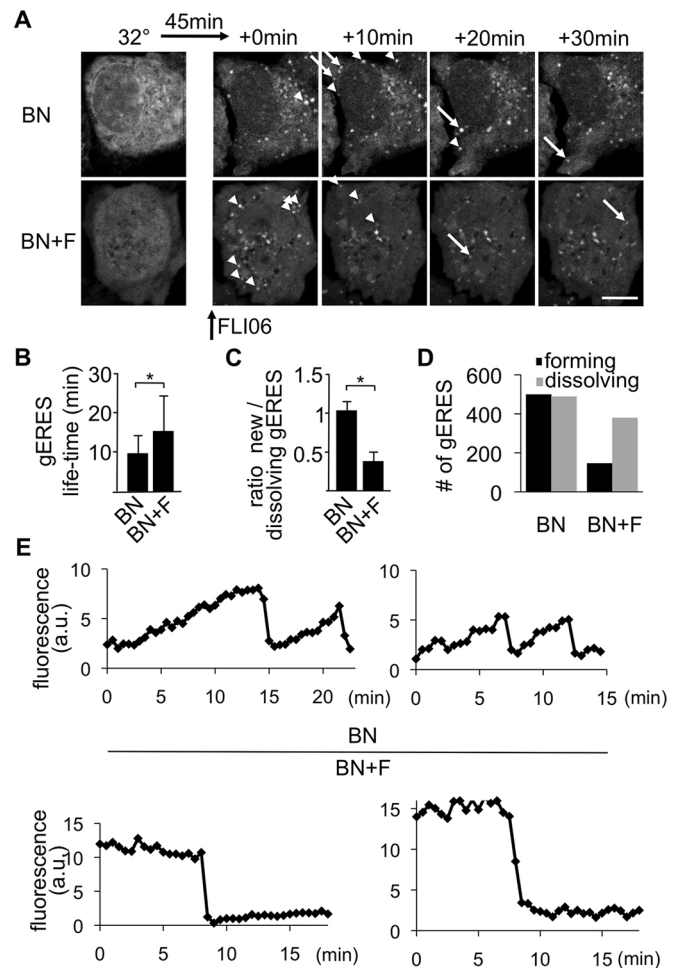


Fig. 3. FLI-06 does not disrupt existing VSVG–EYFP-containing ERES.

(A) HeLa cells transiently transfected with VSVG–EYFP were incubated overnight at 40°C to accumulate VSVG–EYFP in the ER. Cells were then incubated on ice for 30 min with 5 µg/ml BFA and 1 µg/ml nocodazole (denoted BN) and chased in this BFA- and nocodazole-containing medium for indicated times at 32°C. FLI-06 (10 µM) was added after 45 min at 32°C (denoted BN+F). DMSO served as control. Live-cell imaging was performed by acquiring images every 10 s. Single frames from selected sequences are shown. Arrows depict newly forming gERES, arrowheads highlight dissolving gERES. Scale bar: 10 µm. (B) The mean±s.d. life-time of gERES in the presence of BFA, nocodazole and DMSO (BN), or BFA, nocodazole and FLI-06 (BN+F) from A were determined. 81 (BN) and 44 (BN+F) gERES from four and three independent experiments, respectively, were measured. * $P<0.05$ (Student's t -test). (C) The ratio of the number of newly forming to dissolving gERES was determined from 45-min-long time-lapse sequences started after 45 min at 32°C±FLI-06 in the conditions as in A and B. Data are from 8 (BN) and 10 (BN+F) cells from four or three independent experiments, respectively. The error bar reflects s.d. * $P<0.05$ (Student's t -test). (D) Absolute numbers of forming and dissolving gERES from C. (E) Intensity profiles over time of single gERES of VSVG–EYFP-transfected HeLa cells treated as in A. Top, two typical examples of gERES in BFA and nocodazole (BN)-treated cells; bottom, two typical examples of gERES in BFA, nocodazole and FLI-06 (BN+F)-treated cells. A.u., arbitrary units.

ERES, not the capture of cargo in ERES. This suggests the existence of a pre-ERES sorting or concentration mechanism.

FLI-06 inhibits exit from the TGN

We showed in the original characterization of FLI-06 that it inhibited ER export, but whether it would also block later transport steps was not analyzed (Krämer et al., 2013). Transport out of the

TGN can be inhibited by incubation at 20°C (Matlin and Simons, 1983); therefore, a combination of 40°C followed by 20°C incubation allows accumulation of VSVG in the TGN. A subsequent shift to 32°C enables the analysis of post-Golgi export. HeLa cells transfected with VSVG–EYFP were incubated overnight at 40°C and VSVG–EYFP was either chased directly to the plasma membrane or first to the TGN from where it was chased to the plasma membrane in the presence or absence of FLI-06 (Fig. 4A). Transport to the plasma membrane was quantified by determining the ratio of total (EYFP) fluorescence to surface (sVSVG) fluorescence (Fig. 4B). Chasing VSVG–EYFP directly from the ER to the plasma membrane resulted in a threefold increase in surface-to-total ratio, whereas incubation for 2 h at 20°C resulted in accumulation of VSVG–EYFP at the TGN. In the presence of DMSO as control, efficient transport from the TGN to the plasma membrane occurred upon the shift to 32°C, comparable to levels obtained by direct chase. In contrast, transport of VSVG–EYFP from the TGN to the plasma membrane was strongly reduced when cells were treated with FLI-06, and VSVG–EYFP was still observed in the TGN after 2 h at 32°C (Fig. 4A,B). To further substantiate these findings, we employed HeLa cells stably expressing a secreted alkaline phosphatase (SEAP). SEAP release into the medium is reflected by an increase in activity over time that can be inhibited by FLI-06 (Fig. 4C). To monitor post-Golgi transport, SEAP cells were subjected to a 2-h 20°C incubation and chased at 37°C for 60 min. Protein synthesis was inhibited by cycloheximide. FLI-06, but not DMSO, inhibited post-Golgi secretion of SEAP (Fig. 4D). EC_{50} rates for inhibition of ER and TGN exit were determined to be

$2\pm 0.1\ \mu\text{M}$ and $1.4\pm 0.3\ \mu\text{M}$ (mean \pm s.d.), respectively. The EC_{50} value of ER exit is in line with previous results (Krämer et al., 2013), whereas the EC_{50} for TGN exit is slightly reduced, suggesting TGN exit is slightly more sensitive to FLI-06.

Taken together, these data suggest that FLI-06 inhibits not only ER exit, but also TGN exit, suggesting that there is a common cargo recruitment mechanism in both organelles.

FLI-06 acts upstream of Sar1

Could Sar1 be the target of FLI-06 at the ER? Sar1 is thought to be recruited to the ER by Sec12 before cargo recruitment. Inhibition of Sar1 results in a similar phenotype to that seen upon FLI-06 treatment: no concentration of VSVG, no export out of the ER and disruption of the Golgi (Aridor et al., 2001; Kuge et al., 1994). Sar1 is thought to play a dual role in ER export. After recruitment to ER membranes by Sec12, GTP-binding induces membrane curvature and Sec23–Sec24 recruitment. After complete recruitment of the COPII coat, fission is initiated by GTP hydrolysis (reviewed in Zanetti et al., 2011). Our previous data showed that *in vitro* COPII budding, essentially dependent on Sar1 (Barlowe et al., 1994), is not inhibited by FLI-06, arguing against it being the target (Krämer et al., 2013). To make sure that Sar1 indeed is not the target, we further analyzed the mechanism of FLI-06 in cells. If FLI-06 indeed does not inhibit Sar1, the export of VSVG out of ERES should not be blocked. To demonstrate this, VSVG–EYFP was accumulated in gERES with nocodazole and Golgicide A, a drug with the same target as BFA (GBF1, Saenz et al., 2009) but better washout properties (our observations). After washout, the VSVG–EYFP that

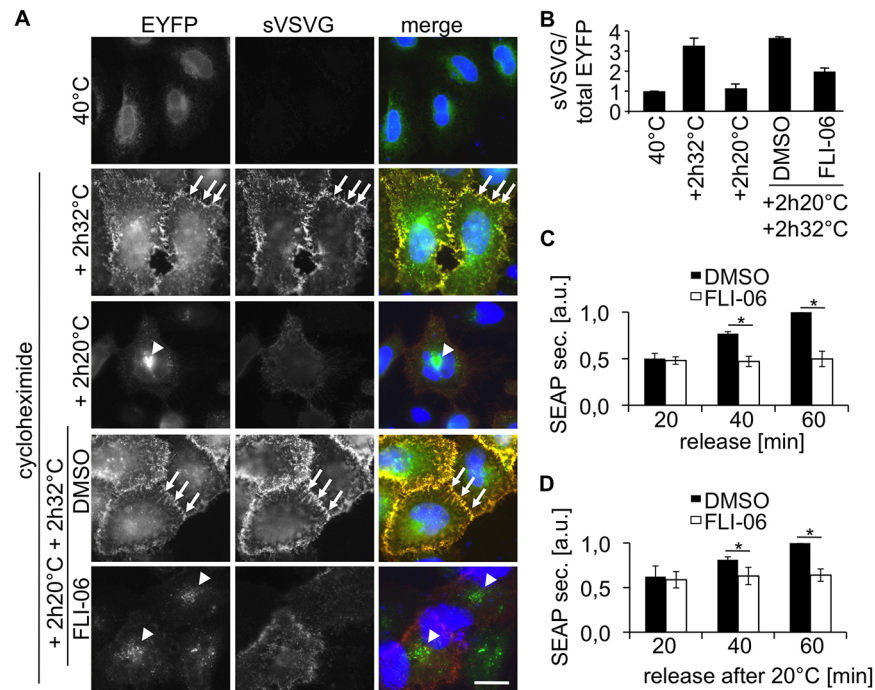


Fig. 4. FLI-06 inhibits post-Golgi transport. HeLa cells transfected with VSVG–EYFP were incubated overnight at 40°C, followed by 2 h at 20°C to chase VSVG–EYFP to the TGN, or directly chased at 32°C. Exit out of the TGN was then monitored at 32°C for 2 h in the presence of 10 μM FLI-06 or DMSO, both added by 10 min before end of the 20°C block. Cycloheximide was present throughout the 20°C and 32°C treatments. VSVG at the surface (sVSVG) was visualized by cell surface staining with anti-VSVG antibody. Arrowheads point to the TGN, arrows to the plasma membrane. Exposure times and processing for sVSVG were identical in all conditions. Representative cells from at least $n=3$ independent experiments are shown. Scale bar: 10 μm . (B) Quantification of three independent experiments as in A. Displayed is the mean \pm s.e.m. ratio of surface VSVG–EYFP (sVSVG) labeling versus total VSVG–EYFP staining. The ratio after 40°C overnight incubation was set to 1 and the other values are presented relative to that value. (C,D) HeLa cells stably expressing SEAP were incubated in fresh medium for indicated times in DMSO or 10 μM FLI-06. In D cells were additionally incubated for 2 h at 20°C to accumulate SEAP in the TGN. FLI-06 or DMSO were added by 10 min before end of the 20°C block. Cycloheximide was present throughout the 20°C and 32°C treatments. Media were collected, SEAP activity determined and the data from three independent experiments displayed as means \pm s.e.m. * $P<0.05$ (Student's *t*-test).

pre-accumulated in gERES was exported to the Golgi in the presence and absence of FLI-06, confirming the *in vitro* data of the COPII-budding assay (Fig. 5A; Movie 2). Quantification using overlap coefficients clearly showed that, in the presence of FLI-06, VSVG–EYFP translocated from gERES to the Golgi within 45 min (Fig. 5B; Fig. S1A). Later steps in cargo release from the ERES to ERGIC are therefore not affected. Note that in the presence of FLI-06, VSVG–EYFP moves to the Golgi, but not further down the secretory pathway because FLI-06 also blocks TGN exit (Fig. 4). To further rule out a potential connection of Sar1 and FLI-06 we made use of H89, a kinase inhibitor known to prevent Sar1 recruitment to ERES membranes (Aridor and Balch, 2000; Nakagawa et al., 2012). We also used EGFP-tagged wild-type (wt) and dominant-negative Sar1b mutants T39N or H79G, that are restricted to the GDP or GTP state, respectively (Aridor et al., 1995; Kuge et al., 1994). HeLa cells

transfected with prlss-KDEL-mRFP as an ER marker and additionally transfected with Sar1 variants were compared by live-cell microscopy with cells transfected with ER marker only with and without FLI-06 or H89 (Fig. 6A,B). As shown previously, FLI-06 caused the ER to completely lose its tubular network and convert into sheets, whereas neither H89, Sar1wt nor Sar1T39N or Sar1H79G changed ER morphology. Given that structure–activity relationships showed that the ER morphology change is tightly associated with ER export inhibition by FLI-06 function (Krämer et al., 2013), this suggests that the FLI-06 target and Sar1 are not in the same pathway. Fig. 6C demonstrates that FLI-06 redistributes Sec31-labeled ERES from perinuclear to more peripheral punctate structures, without reducing the number of punctate ERES. In contrast, treatment with H89 for 2 h drastically reduced the number of ERES and resulted in an increase in cytosolic Sec31 (Fig. 6C, thick arrow). Overexpression of EGFP-tagged Sar1wt and Sar1T39N resulted in a reduction of punctate ERES numbers that was more pronounced in Sar1H79G-expressing cells (Fig. 6D). As described before (Ward et al., 2001), in Sar1H79G-expressing cells Sec31 and Sar1 colocalized in bigger fragmented Golgi-like structures (Fig. 6D). Functionality of Sar1 mutants was assessed by testing their capability to disrupt the Golgi (Fig. S1B). Quantification of ERES numbers confirmed that both H89 and transfection with Sar1 constructs but not FLI-06 reduced the mean ERES number per cell (Fig. 6E). In agreement with this, FLI-06 did not change the distribution of the ERES markers Sec16B, Sec24 and TFG (Fig. S2A). In addition, stimulated emission depletion (STED) microscopy showed that the close proximity of TFG1 to Sec31 is not affected by FLI-06 (Fig. S2B). These data show that the FLI-06 phenotype is different from phenotypes caused by H89 or Sar1 mutants, suggesting Sar1 is not the target of FLI-06. Interestingly, ERES fully equipped with the COPII machinery persisted, although no new secretory cargo was recruited and exit of the already concentrated cargo is permitted by FLI-06.

Autophagosome biogenesis is induced and ER-peroxisome transport is not affected by FLI-06

The inhibition of ER and TGN export of secretory proteins by FLI-06 suggests mechanisms with at least partly common components that might govern all vesicular budding events. We therefore analyzed other ER export pathways, namely transport to peroxisomes (Hoepfner et al., 2005) and generation of autophagosomes (Ge et al., 2013; Graef et al., 2013; Zoppino et al., 2010). In these cases, the ER provides at least some proteins and lipids and ERES are involved (reviewed in Sanchez-Wandelmer et al., 2015; Tabak et al., 2013). To analyze transport to peroxisomes, we made use of pex16–EGFP and ss-pex3–EGFP. The former is a membrane protein that transits through the ER to peroxisomes (Kim et al., 2006), the latter is forced through its artificial signal sequence to first enter the ER before it is transported to peroxisomes (Aranovich et al., 2014). HeLa cells were transfected with pex16–EGFP and ss-pex3–EGFP and incubated with FLI-06 after 2 h, before the first EGFP-labeled peroxisomes could be detected (Fig. 7). After 20 h, both constructs labeled numerous peroxisomes in all conditions, indicating that the ER export route to peroxisomes is independent of an FLI-06-sensitive machinery (Fig. 7A). The disruption of the Golgi, stained by anti-giantin antibodies, indicated FLI-06 efficacy. Similarly, the generation of autophagosomes, visualized by antibodies against endogenous LC3, is also not inhibited by FLI-06, but rather induced twofold after 4 h. A combination of Torin and Bafilomycin served as a positive control (Fig. 7B,C). Taken together, these data suggest

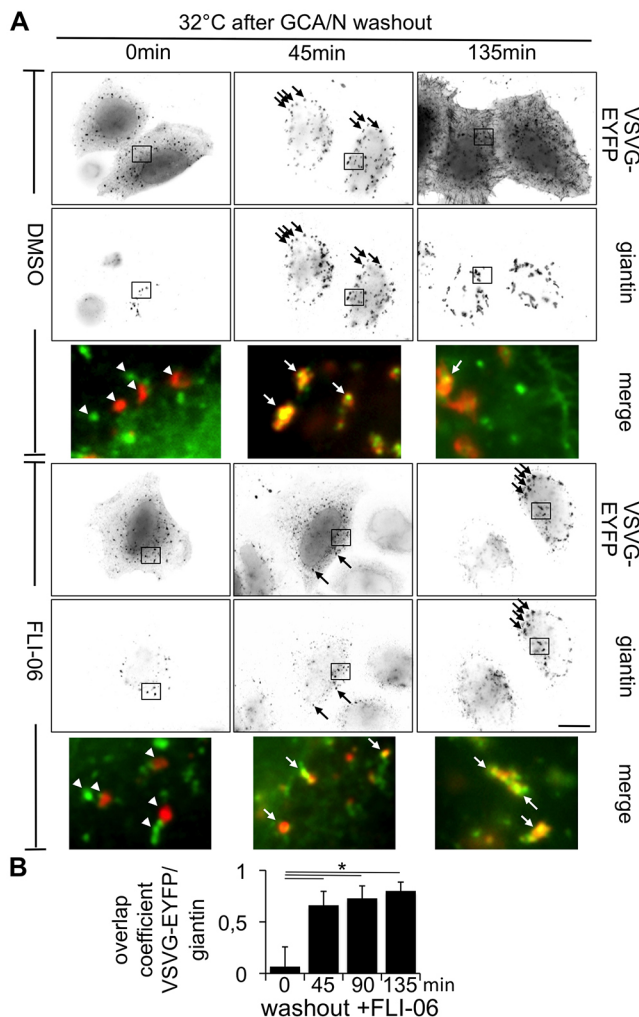


Fig. 5. FLI-06 does not inhibit export out of preexisting ERES. HeLa cells transfected with VSVG–EYFP were incubated overnight at 40°C, followed by 45 min with 10 μ M GCA and 1 μ g/ml nocodazole (GCA/N) at 32°C to induce gERES. After washout, cells were incubated for indicated times at 32°C with or without 10 μ M FLI-06, fixed and processed for immunofluorescence with anti-giantin antibodies. (A) Shown are inverted images, with enlargements of the boxed areas as color merges. Arrows indicate colocalization; arrowheads no colocalization. Representative cells from at least $n=3$ independent experiments are shown. Scale bar: 10 μ m. (B) Overlap coefficient of VSVG–EGFP and giantin fluorescence from 37–61 cells/timepoint from three independent experiments of with GCA/N washout in the presence of FLI-06. * $P<0.05$ (one-way analysis of variance followed by Dunnett's multiple comparison test).

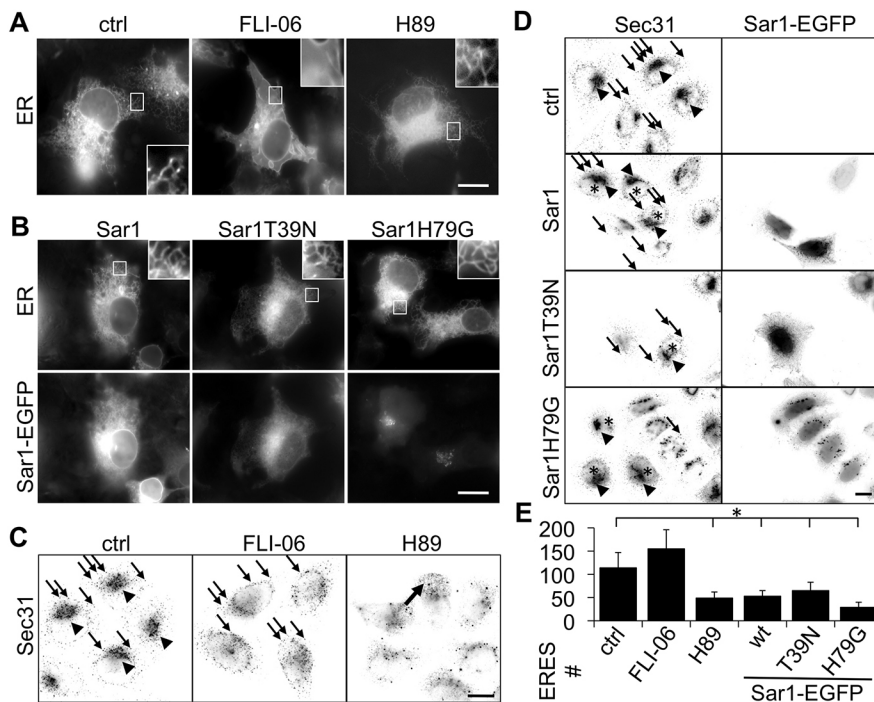


Fig. 6. FLI-06 does not inhibit Sar1 function and preserves ERES. HeLa cells plated in Labtek chambered coverglass were transfected with prlss-KDEL-mRFP (A,B) and additionally with Sar1-EGFP mutants (B) for 24 h where indicated. 10 μ M FLI-06 or 100 μ M H89 was added for >30 min. Images were taken from living cells. The boxed areas are enlarged to show ER morphology. HeLa cells were treated with 10 μ M FLI-06 or 100 μ M H89 for 2 h (C) or transfected with Sar1-EGFP mutants for 24 h (D), fixed and processed for immunofluorescence with anti-Sec31 antibodies. Inverted images are shown. Arrowheads, centrally located ERES; arrows, peripheral punctate ERES; asterisks, untransfected cells; thick arrow, cytoplasmic Sec31. Representative cells from at least $n=3$ independent experiments are shown. (E) Mean \pm s.d. ERES number (#) per cell in treatments from C and D as indicated. $n>40$ cells/condition from three or four independent experiments. Scale bar: 10 μ m. * $P<0.05$ (one-way analysis of variance followed by Holm–Sidak method).

that FLI-06 specifically inhibits ER-to-Golgi transport, not transport to peroxisomes. Biogenesis of autophagosomes is also not inhibited, but in contrast is induced by FLI-06.

FLI-06 inhibits exocytic, not endocytic traffic

We showed previously that FLI-06 does not inhibit uptake from the plasma membrane to early endosomes (Krämer et al., 2013) but we did not analyze whether later endocytic transport steps would be inhibited. To further analyze the potential impact of FLI-06 on endocytic pathways, we investigated uptake of transferrin to late endosomes. To this end, HeLa cells were incubated with Alexa-Fluor-labeled transferrin for 30 min on ice in the presence or absence of FLI-06, followed by a medium change and a chase at 37°C for up to 60 min (Fig. S3). Surface transferrin was stripped to visualize only the internalized transferrin. In both conditions, at 15 min of chase numerous early endosomes were visible in the periphery of the cells, which after 60 min were mostly concentrated in a juxtanuclear position, indicative of late endosomes. This data suggest that uptake to early endosomes and transport to late endosomes are not inhibited by FLI-06.

DISCUSSION

A vast amount of data has been generated since George Palade described the organelles of the secretory pathway and the vesicular traffic from the ER to the plasma membrane (Palade, 1975). Many of the involved protein complexes, including SNARE proteins, COPI and COPII coats were described, and the molecular mechanisms elucidated. All that culminated in the awarding of the Nobel prize 2014 to J. Rothman, R. Schekman and T. Südhof. However, many questions still remain unsolved or are unclear. For example, the first steps of cargo selection and concentration in future budding areas are not very well defined. The current models of ER exit state that the initial Sar1–Sec12 interaction, probably at ERES defined by Sec16, is coupled to cargo recruitment through Sec23–Sec24, followed by Sec13–Sec31 recruitment (Budnik and Stephens, 2009; Venditti et al., 2014; Zanetti et al., 2011). To what

extend ERES preexist without cargo, if and how cargo needs to be recruited to ERES before the Sar1 and COPII machinery takes over, and what the spatial arrangement of ERES and the COPII machinery are, are all open questions. Some additional mechanisms of cargo recruitment have been unraveled in the case of large cargo proteins like procollagen that do not fit into normal sized COPII vesicles. Here, special adaptors like TANGO1, sedlin and cTAGE5 guide procollagen to ERES and help to pack them in specialized large COPII vesicles (Jin et al., 2012; Saito et al., 2009, 2011; Venditti et al., 2012). Whether similar concentration and recruitment mechanisms upstream of Sar1 and COPII exist for all secretory cargo is an open question. According to the prevailing model, COPII components would not be recruited to ERES in the absence of cargo. Our experiments strongly suggest that, first, there must be an active recruitment to or concentration in ERES for all proteins that leave the ER, not only for the very bulky ones. Cargo does not just diffuse into ERES. Second, the COPII machinery at ERES is present in the absence of cargo recruitment. Third, FLI-06 specifically inhibits the recruitment or concentration of cargo to ERES and does not simply immobilize cargo in the ER membrane (our FRAP data). Our time-lapse experiments demonstrate that preexisting cargo recruitments in ERES are not dissolved by FLI-06, but new recruitments are blocked. This demonstrates that FLI-06 does not inhibit the capture of cargo to Sec23–Sec24 nor its export to the Golgi once it is in ERES. Given that new recruitment is blocked, we expected that with the export of the remaining cargo the COPII machinery is consumed, but instead ERES containing Sec16, Sec24, Sec31 and TFG1 are still present in FLI-06 treated cells. We showed previously that FLI-06 inhibits not only ER export of membrane proteins but also of secreted and GPI-anchored proteins (Krämer et al., 2013). The data therefore suggest that, in contrast to the current models, COPII components are associated with ERES in a cargo-independent manner and might fulfill additional functions beyond generating COPII vesicles. Alternatively, persistent COPII at ERES might be engaged in non-secretory transport routes, for example to peroxisomes (see below). However, assuming that

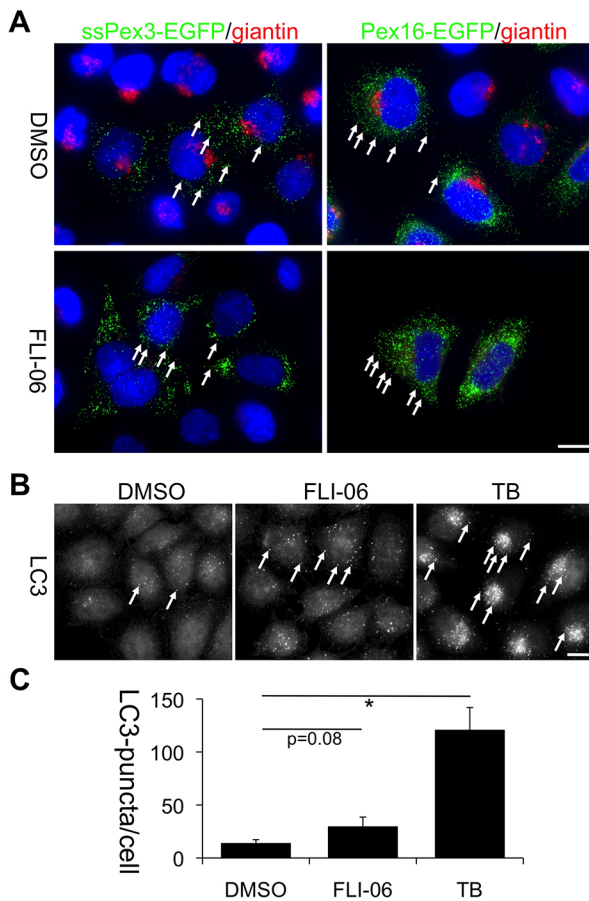


Fig. 7. Transport from ER to peroxisomes and generation of autophagosomes are not inhibited by FLI-06. (A) HeLa cells were transfected with ssPex3–EGFP or Pex16–EGFP and 10 μ M FLI-06 was added 2 h after transfection, before EGFP-labeled peroxisomes are detectable. After 20 h cells were fixed, processed for immunofluorescence with anti-giantin antibodies and imaged by fluorescence microscopy. The dispersal of the Golgi in FLI-06 treated cells shows its efficacy. (B) Autophagy is induced, not inhibited by FLI-06. HeLa cells were treated with DMSO or 20 μ M FLI-06 or with 250 nM Torin plus 200 nM Bafilomycin (denoted TB) for 4 h, fixed, processed for immunofluorescence with antibodies against endogenous LC3B and imaged by fluorescence microscopy. Arrows point to LC3B-positive autophagosomes. Scale bar: 10 μ m. (C) Quantification of LC3B-positive puncta in cells from B. Displayed is the mean number of LC3B puncta per cell from 205 (DMSO), 185 (FLI-06) and 253 (TB) cells from $n=3$ independent experiments. * $P<0.05$ (Student's *t*-test).

secretory transport comprises a major, if not the largest fraction of ER export, it is surprising to not at least see a reduction in COPII at ERES. FLI-06 seems to disrupt the feedback mechanisms shown previously to modulate ERES number depending on cargo load (Farhan et al., 2008). This might be because this feedback involves the unfolded protein response (UPR) (Farhan et al., 2008), which is only mildly upregulated in FLI06-treated cells (Krämer et al., 2013).

Interestingly, at the ER, FLI-06 specifically blocks recruitment to ERES but not export to other destinations, like autophagosome biogenesis or transport routes from the ER to peroxisomes. This is especially intriguing given that these pathways share at least some components of the COPII machinery with secretory ER export (Ge et al., 2014, 2013; Yonekawa et al., 2011; Graef et al., 2013; Hoepfner et al., 2005; Kim et al., 2006; Soni et al., 2009; Zoppino et al., 2010). Interestingly, FLI-06 induces autophagy, but whether

it affects selective or non-selective autophagy or ER-phagy (selective degradation of the ER) remains to be shown in future studies.

Our data support a model of active cargo recruitment to ERES, involving a specific protein or lipid that is inhibited by FLI-06. Such a factor could be a recruitment factor that binds cargo and actively transports it into ERES, but it could also be a watchdog that has to be removed or modified in order to let cargo pass and enter into ERES. FLI-06 would then inhibit the opening mechanisms, blocking all access into ERES. Our data do not support a model where cargo freely enters and exits ERES and is concentrated through protein–protein interactions in ERES.

Surprisingly, exit of secretory cargo out of the ER and the TGN must be governed by similar mechanisms, given that FLI-06 inhibited both pathways, but left others like endocytosis, early-to-late-endosome transport as well as ER-peroxisome and autophagosome biogenesis intact. No clear TGN exit sites have been identified, where cargo is recruited and vesicles bud off (Kienzle and von Blume, 2014). Whether FLI-06 acts at the TGN through similar mechanisms like in ERES or, alternatively, is an indirect effect, remains an open question and needs methodological development of current assays.

Sar1 and its GTPase activity are essential for COPII vesicle formation (reviewed in Aridor and Balch, 2000; Nakagawa et al., 2012; Venditti et al., 2014; Zanetti et al., 2011). Could Sar1 be the target of FLI-06? We cannot rule out this possibility, but several observations argue for a role of FLI-06 upstream of Sar1. First, FLI-06 has no direct effect in a COPII *in vitro* budding assay (Krämer et al., 2013) and did not inhibit exit of pre-accumulated VSVG–EYFP from ERES. Sar1 controls not only assembly but also fission of COPII vesicles (Long et al., 2010); therefore, if Sar1 is the target, FLI-06 would inhibit export of pre-accumulated cargo. Second, in contrast to FLI-06 treatment, overexpressing Sar1 and two inactive Sar1 mutants caused a reduction in number of ERES, but not a conversion in morphology from ER tubules to sheets, again suggesting FLI-06 does not act through Sar1. Third, the unspecific kinase inhibitor H89, known to dissociate Sar1 from ER membranes (Aridor and Balch, 2000; Nakagawa et al., 2012), causes a dramatic downregulation in Sec31-labeled ERES not seen with FLI-06 and no tubular-sheet transformation of the ER, again arguing that FLI-06 does not act on Sar1.

In conclusion, we propose a model, where a hitherto unknown factor X is essential for cargo to be concentrated in ERES and the TGN. In ERES this factor acts prior to the Sar1 and COPII machinery. This machinery is present in the absence of cargo, suggesting it fulfills additional functions beyond vesicle biogenesis. Future work aims at identifying the molecular target of FLI-06 and elucidation of its function.

MATERIALS AND METHODS

Antibodies and cell lines

The following antibodies were used. Rabbit anti-LC3B (MAP1LC3B antibody; 1:1000; PM036, MBL); mouse anti-Sec31a (1:500, #612350, BD); mouse anti-giantin (1:500, ALX-804-600, Enzo); mouse anti-VSVG 8G5F11 (1:200, EB0010, Kerafast) and folding-specific anti-VSVG IE9F9 (1:200 for immunofluorescence, 1:1000 for western blotting; EB0012, Kerafast). Alexa-Fluor-488-, -555- or -586-labeled secondary antibodies were used at 1:500 dilution (Invitrogen). Unauthenticated HeLa-Kyoto cells were obtained from Rainer Pepperkok (EMBL Heidelberg, Germany) and grown in Dulbecco's modified Eagle's medium (DMEM) supplemented with 10% fetal calf serum (FCS) in standard conditions (5% CO₂, 37°C).

Compounds

If not indicated otherwise, all compounds were from Sigma Aldrich. GCA was from Calbiochem, Torin from R&D Systems, Bafilomycin from Abcam. FLI-06 was synthesized as described previously (Krämer et al., 2013).

cDNA constructs and transfections

VSVG–EYFP is as described in Toomre et al. (1999) with the linker DPPVAT, but with the EGFP replaced by an EYFP. VSVG refers to VSVGtsO45 (Gallione and Rose, 1985) throughout the manuscript. NS5A–GFP as described in Nevo-Yassaf et al. (2012). Pex3–GFP and ss-Pex3–GFP (Aranovich et al., 2014) were kindly provided by Peter Kim, Toronto, Canada. GFP–TFG and mCherry–Sec16B were kindly provided by Jon Audhya (University of Wisconsin, Madison, USA) (Witte et al., 2011). The ER marker prlss-KDEL-mRFP (Snapp et al., 2006) was kindly provided by Erik Snapp (Albert Einstein College of Medicine, New York, USA). Cells were transiently transfected using Lipofectamine (Invitrogen).

Transferrin uptake

After starving cells for 6–8 h in serum-free medium, cells were washed two times on ice with pre-cooled serum-free medium before labeling on ice in 25 µg/ml transferrin–Alexa-Fluor-555 (Invitrogen). After 15 min, cells were washed in serum-free medium and incubated at 37°C for various times. Before fixation in Roti-Histofix (Roth), surface transferrin was removed by washing two times in PBS, adding stripping solution (150 mM NaCl, 2 mM CaCl₂, 25 mM CH₃COONa, pH 4.5) for 5 min and washing again two times in PBS. After staining nuclei with DAPI, fixed cells were mounted in mowiol.

Autophagosome and peroxisome labeling

To monitor autophagy, HeLa cells seeded on cover slips were incubated with DMSO, FLI-06, or Torin and Bafilomycin, fixed and prepared for immunocytochemistry with anti-LC3B antibodies. To label peroxisomes, HeLa cells were transfected with Pex3–GFP and ss-Pex3–GFP (Aranovich et al., 2014), and FLI-06 or DMSO was added after 4 h, before the appearance of GFP-labeled peroxisomes. After 20 h, cells were fixed and stained with anti-giantin antibodies and Hoechst 33258 or DAPI.

Surface VSVG staining

Cells were washed twice with PBSI (PBS plus 1 mM CaCl₂, 0.5 mM MgCl₂, pH 7.4), then incubated with anti-VSVG Kerafast 8G5F11 (2 µg/ml) in PBSI for 30 min on ice. Cells were washed with PBSI three times, then fixed with histofix for 5 min on ice and 20 min at room temperature. Cells were then washed three times with PBS, and incubated with 1% BSA in PBS for 20 min. Thereafter anti-mouse-IgG conjugated to Alexa Fluor 555 (1:500 dilution in 0.1% BSA in PBS) was added for 20 min. Cells were washed again twice with PBS. After staining nuclei with Hoechst 33258, fixed cells were mounted in mowiol. The surface to total VSVG ratio was determined using a Celloomics Arrayscan (Thermo Fisher). The position and area of the nucleus was determined using the Hoechst 33258 staining, and fluorescence intensities of EYFP (total) and Alexa Fluor 555 (surface VSVG) was determined in an area covering the nuclear area plus a ring of 2–3 µm around the nucleus, and the surface-to-total ratio was calculated.

SEAP assay

SEAP (human ALPP, gene ID 250) from plasmid CMV-SEAP (Addgene #24595) was subcloned into pCDNA3.1 Hygro, transfected in HeLa cells, and stably expressing SEAP cells selected by hygromycin treatment. To measure SEAP secretion, cells in 96-well plates were washed two times with PBS and incubated in serum-free DMEM for the indicated times. Supernatants were transferred to new 96-well plates, covered with foil and heated for up to 65°C for 20 min. Afterwards, 75 µl SEAP buffer (100 mM Tris-HCl, pH 9.5, 100 mM NaCl, 20 mM MgCl₂) containing 2 mg/ml p-nitrophenyl phosphate (pNPP) was added and the plates were incubated at 37°C for 19 h. Absorbance was measured at 405 nm using a Mithras LB 940 Multimode Microplate Reader.

Induction of gERES and live-cell imaging

HeLa cells transiently transfected with VSVG–EYFP were incubated overnight at 40°C to accumulate VSVG–EYFP in the ER. Cells were then

incubated on ice for 30 min with 5 µg/ml BFA and 1 µg/ml nocodazole followed by incubation for 45 min at 32°C to induce gERES. Cells were fixed after further incubation at 32°C for 45 and 90 min with or without 10 µM FLI-06. For washout experiments, 10 µM GolgicideA (GCA) was used instead of BFA, and after incubation for 45 min at 32°C cells were intensely washed by three wash steps in PBS before further incubation as indicated. For live-cell imaging, HeLa cells were transiently transfected with VSVG–EYFP, incubated overnight at 40°C, then placed on ice for 30 min with 5 µg/ml BFA and 1 µg/ml nocodazole. Thereafter, cells were incubated for indicated times on stage in a microscope incubator housing (XL 2000 PeCon) which was kept at 32°C by Heating Unit XLS (PeCon). Live images were taken using an Axio Observer Z1 microscope (Carl Zeiss) with Definite Focus (Carl Zeiss) and a Plan Apochromat 63×, 1.40 NA oil objective attached to a spinning disk confocal unit (CSU-X1; Yokogawa electric corporation) and frames were taken every 10 s by an Evolve 512 camera (Photometrics) in the presence or absence of 10 µM FLI-06. Prewarmed Leibovitz's L-15 medium was used instead of DMEM for live-cell imaging. For quantification, stacks were imported into ImageJ and the lifetime of gERES and the numbers of newly formed and dissolving gERES was manually analyzed [total number of ERES forming and disappearing, respectively, were 500 and 489 in cells treated with BFA and nocodazole (control, BN), and 147 and 380 in cells treated with BFA, nocodazole and FLI-06 (BNF)]. The pixel fluorescence variances (PFV) was determined as described previously (Dukhovny et al., 2008; Krämer et al., 2013). Fluorescence intensity profiles of single gERES were determined from time-lapse movies using ImageJ.

Microscopy

Immunofluorescence was performed using standard protocols (Wacker et al., 1997). For ER morphology analysis, COS7 cells in LabTek chambered coverglass were transfected with prlss-KDEL-mRFP (Snapp et al., 2006) for 24 h and imaged alive with or without compound treatment. Fluorescence microscopy was performed on Zeiss Axiovert or Axio Imager microscopes using 63×1.4 NA objectives and Axiovision or ZEN software (Zeiss). FRAP experiments were performed on a confocal microscope (LSM 710 Meta; Carl Zeiss, Inc.) essentially as described before (Diekmann and Hoischen, 2014; Hemmerich et al., 2008) using a C-Apochromat infinity-corrected 1.2 NA 40× water objective and the 514-nm laser line for YFP. Five images were taken before the bleach pulse and 120 images after bleaching (30 iterations with 100% laser intensity) of a rectangular region, which was for all experiments of the same size and shape, covering a small area of the nuclear membrane. The image acquisition frequency was set to 0.5 frames/s at 0.3% laser transmission, a zoom of 5 and a pixel dwell time of 3.15 µs. During the FRAP experiments, the pinhole was set to 2.5 Airy Units. Quantification of relative fluorescence intensities was performed using Sigma Plot software. Recovery half-times and residence times were determined from FRAP data as described previously (Schmiedeberg et al., 2004). All super-resolution images were acquired on a Leica TCS SP8 STED-3X equipped with an inverted microscope (DMI 8, Leica) and a 100× STED objective (HC PL APO CS2 100×1.4 oil STED, Leica). For STED, fixed HeLa cells transfected with VSVG–EYFP were stained with anti-Sec31 and -GFP antibodies and with Abberior STAR 580 and 635p secondary antibodies. STED images were acquired sequentially between frames using a 583 nm laser line for Abberior STAR 580 and a 633-nm laser line for Abberior STAR 635P. Abberior STAR 580 was detected by using HyD SP GaAsP detector 2 (HyD timegate=0.7 ns–5.9 ns; gain=100) of the spectral detection unit with the detection range set to 589–617 nm and Abberior STAR 635p was detected on the same detector (HyD timegate=0.7 ns–5.9 ns; gain=130) with the detection range set to 642–700 nm. Imaging speed was at 400 Hz using 6× line averaging and 2–3× frame Accu. The pinhole was set to 0.9 Airy units (141 µm). At zoom 3.3 and a format of 3688×1844, the resulting pixel size was 11 nm. The pulsed 775-nm depletion laser (1.5 W; output=100%) was activated to 90% for stimulated emission depletion for Abberior STAR 580 and to 100% for Abberior STAR 635p. We estimated the xy resolution limit of our STED system to be ~45 nm by measuring the full-width half maximum of the obtained images using Leica's LASAF quantification tool.

Image analysis

For colocalization analysis, the coloc tool in Zen (Zeiss) was used. Coloc calculates the overlap coefficient according to Manders et al. (1993) and generates scatter plots as in Fig. S1A. Sec31-labeled ERES and LC3B puncta were quantified using CellProfiler (www.cellprofiler.org, Kametsky et al., 2011). Detection thresholds were applied for each experimental set to adapt to variation in background intensities. ERES numbers in FLI-06-treated cells are probably overestimated compared to in the DMSO control, because of the redistribution of ERES from their compact, difficult to count individually, juxtanuclear localization to an even distribution throughout the cell.

Statistical analysis

Data are presented as mean±s.e.m. or s.d. as indicated. The number of independent experiments (*n*) is indicated. Paired or unpaired Student's *t*-test or one-way analysis of variance followed by Dunnett's multiple comparison test was applied to evaluate differences between experimental groups.

Acknowledgements

We thank Peter Kim for pex-plasmids and helpful suggestions, Erik Snapp and Jon Audhya for plasmids, and Rainer Pepperkok for HeLa-Kyoto cells. We are grateful for support from the FLI imaging and functional genomics facilities.

Competing interests

The authors declare no competing or financial interests.

Author contributions

Y.Y., X.L., K.M., A.K., T.M., P.A., T.F., T.K. performed cell biological experiments and analysis. C.H. and P.H. performed FRAP and STED experiments and analysis, Y.Y. and O.S. performed live-cell imaging and data analysis. R.N. and H.-D.A. synthesized FLI-06. C.K. designed experiments, and C.K. and K.H. discussed the data and wrote the manuscript with the help of all authors. All authors discussed the results and implications at all stages.

Funding

This work was supported by a grant from the Deutsche Forschungsgemeinschaft [grant number KA1751/4-1 to C.K.], the Japan Society for the Promotion of Science (to Y.Y.) and Israel Science Foundation [grant number 1533/12 to K.H.].

Supplementary information

Supplementary information available online at <http://jcs.biologists.org/lookup/doi/10.1242/jcs.186163.supplemental>

References

- Aranovich, A., Hua, R., Rutenberg, A. D. and Kim, P. K. (2014). PEX16 contributes to peroxisome maintenance by constantly trafficking PEX3 via the ER. *J. Cell Sci.* **127**, 3675–3686.
- Aridor, M. and Balch, W. E. (2000). Kinase signaling initiates coat complex II (COPII) recruitment and export from the mammalian endoplasmic reticulum. *J. Biol. Chem.* **275**, 35673–35676.
- Aridor, M., Bannykh, S. I., Rowe, T. and Balch, W. E. (1995). Sequential coupling between COPII and COPI vesicle coats in endoplasmic reticulum to Golgi transport. *J. Cell Biol.* **131**, 875–893.
- Aridor, M., Fish, K. N., Bannykh, S., Weissman, J., Roberts, T. H., Lippincott-Schwartz, J. and Balch, W. E. (2001). The Sar1 GTPase coordinates biosynthetic cargo selection with endoplasmic reticulum export site assembly. *J. Cell Biol.* **152**, 213–229.
- Bannykh, S. I., Rowe, T. and Balch, W. E. (1996). The organization of endoplasmic reticulum export complexes. *J. Cell Biol.* **135**, 19–35.
- Barlowe, C. K. and Miller, E. A. (2013). Secretory protein biogenesis and traffic in the early secretory pathway. *Genetics* **193**, 383–410.
- Barlowe, C., Orci, L., Yeung, T., Hosobuchi, M., Hamamoto, S., Salama, N., Rexach, M. F., Ravazzola, M., Amherdt, M. and Schekman, R. (1994). COPII: a membrane coat formed by Sec proteins that drive vesicle budding from the endoplasmic reticulum. *Cell* **77**, 895–907.
- Bokel, C., Dass, S., Wilsch-Brauninger, M. and Roth, S. (2006). Drosophila Cornichon acts as cargo receptor for ER export of the TGF α -like growth factor Gurken. *Development* **133**, 459–470.
- Budnik, A. and Stephens, D. J. (2009). ER exit sites—localization and control of COPII vesicle formation. *FEBS Lett.* **583**, 3796–3803.
- Castillon, G. A., Watanabe, R., Taylor, M., Schwabe, T. M. E. and Riezman, H. (2009). Concentration of GPI-anchored proteins upon ER exit in yeast. *Traffic* **10**, 186–200.
- Diekmann, S. and Hoischen, C. (2014). Biomolecular dynamics and binding studies in the living cell. *Phys. Life Rev.* **11**, 1–30.
- Dukhovny, A., Papadopoulos, A. and Hirschberg, K. (2008). Quantitative live-cell analysis of microtubule-uncoupled cargo-protein sorting in the ER. *J. Cell Sci.* **121**, 865–876.
- Farhan, H., Weiss, M., Tani, K., Kaufman, R. J. and Hauri, H.-P. (2008). Adaptation of endoplasmic reticulum exit sites to acute and chronic increases in cargo load. *EMBO J.* **27**, 2043–2054.
- Fujita, M., Watanabe, R., Jaensch, N., Romanova-Michaelides, M., Satoh, T., Kato, M., Riezman, H., Yamaguchi, Y., Maeda, Y. and Kinoshita, T. (2011). Sorting of GPI-anchored proteins into ER exit sites by p24 proteins is dependent on remodeled GPI. *J. Cell Biol.* **194**, 61–75.
- Gallione, C. J. and Rose, J. K. (1985). A single amino acid substitution in a hydrophobic domain causes temperature-sensitive cell-surface transport of a mutant viral glycoprotein. *J. Virol.* **54**, 374–382.
- Ge, L., Melville, D., Zhang, M. and Schekman, R. (2013). The ER-Golgi intermediate compartment is a key membrane source for the LC3 lipidation step of autophagosome biogenesis. *Elife* **2**, e00947.
- Ge, L., Zhang, M. and Schekman, R. (2014). Phosphatidylinositol 3-kinase and COPII generate LC3 lipidation vesicles from the ER-Golgi intermediate compartment. *Elife* **3**, e04135.
- Graef, M., Friedman, J. R., Graham, C., Babu, M. and Nunnari, J. (2013). ER exit sites are physical and functional core autophagosome biogenesis components. *Mol. Biol. Cell* **24**, 2918–2931.
- Guo, Y., Sirkis, D. W. and Schekman, R. (2014). Protein sorting at the trans-Golgi network. *Annu. Rev. Cell Dev. Biol.* **30**, 169–206.
- Hemmerich, P., Weidtkamp-Peters, S., Hoischen, C., Schmiedeberg, L., Erliandri, I. and Diekmann, S. (2008). Dynamics of inner kinetochore assembly and maintenance in living cells. *J. Cell Biol.* **180**, 1101–1114.
- Hoepfner, D., Schildknegt, D., Braakman, I., Philippsen, P. and Tabak, H. F. (2005). Contribution of the endoplasmic reticulum to peroxisome formation. *Cell* **122**, 85–95.
- Jin, L., Pahuja, K. B., Wickliffe, K. E., Gorur, A., Baumgärtel, C., Schekman, R. and Rape, M. (2012). Ubiquitin-dependent regulation of COPII coat size and function. *Nature* **482**, 495–500.
- Kametsky, L., Jones, T. R., Fraser, A., Bray, M.-A., Logan, D. J., Madden, K. L., Ljosa, V., Rueden, C., Eliceiri, K. W. and Carpenter, A. E. (2011). Improved structure, function and compatibility for CellProfiler: modular high-throughput image analysis software. *Bioinformatics* **27**, 1179–1180.
- Kienle, C. and von Blume, J. (2014). Secretory cargo sorting at the trans-Golgi network. *Trends Cell Biol.* **24**, 584–593.
- Kim, P. K., Mullen, R. T., Schumann, U. and Lippincott-Schwartz, J. (2006). The origin and maintenance of mammalian peroxisomes involves a de novo PEX16-dependent pathway from the ER. *J. Cell Biol.* **173**, 521–532.
- Krämer, A., Mentrup, T., Kleizen, B., Rivera-Milla, E., Reichenbach, D., Enzensperger, C., Nohl, R., Täuscher, E., Görls, H., Ploubidou, A. et al. (2013). Small molecules intercept Notch signaling and the early secretory pathway. *Nat. Chem. Biol.* **9**, 731–738.
- Kreis, T. E. and Lodish, H. F. (1986). Oligomerization is essential for transport of vesicular stomatitis viral glycoprotein to the cell surface. *Cell* **46**, 929–937.
- Kuge, O., Dascher, C., Orci, L., Rowe, T., Amherdt, M., Plutner, H., Ravazzola, M., Tanigawa, G., Rothman, J. E. and Balch, W. E. (1994). Sar1 promotes vesicle budding from the endoplasmic reticulum but not Golgi compartments. *J. Cell Biol.* **125**, 51–65.
- Long, K. R., Yamamoto, Y., Baker, A. L., Watkins, S. C., Coyne, C. B., Conway, J. F. and Aridor, M. (2010). Sar1 assembly regulates membrane constriction and ER export. *J. Cell Biol.* **190**, 115–128.
- Manders, E. M. M., Verbeek, F. J. and Aebi, J. A. (1993). Measurement of co-localization of objects in dual-colour confocal images. *J. Microsc.* **169**, 375–382.
- Matlin, K. S. and Simons, K. (1983). Reduced temperature prevents transfer of a membrane glycoprotein to the cell surface but does not prevent terminal glycosylation. *Cell* **34**, 233–243.
- Miller, E. A., Beilharz, T. H., Malkus, P. N., Lee, M. C. S., Hamamoto, S., Orci, L. and Schekman, R. (2003). Multiple cargo binding sites on the COPII subunit Sec24p ensure capture of diverse membrane proteins into transport vesicles. *Cell* **114**, 497–509.
- Nakagawa, H., Ishizaki, M., Miyazaki, S., Abe, T., Nishimura, K., Komori, M. and Matsuo, S. (2012). Sar1 translocation onto the ER-membrane for vesicle budding has different pathways for promotion and suppression of ER-to-Golgi transport mediated through H89-sensitive kinase and ER-resident G protein. *Mol. Cell. Biochem.* **366**, 175–182.
- Nehls, S., Snapp, E. L., Cole, N. B., Zaal, K. J. M., Kenworthy, A. K., Roberts, T. H., Ellenberg, J., Presley, J. F., Siggia, E. and Lippincott-Schwartz, J. (2000). Dynamics and retention of misfolded proteins in native ER membranes. *Nat. Cell Biol.* **2**, 288–295.
- Nevo-Yassaf, I., Yaffe, Y., Asher, M., Ravid, O., Eizenberg, S., Henis, Y. I., Nahmias, Y., Hirschberg, K. and Sklan, E. H. (2012). Role for TBC1D20 and Rab1 in hepatitis C virus replication via interaction with lipid droplet-bound nonstructural protein 5A. *J. Virol.* **86**, 6491–6502.

- Pagant, S., Wu, A., Edwards, S., Diehl, F. and Miller, E. A. (2015). Sec24 is a coincidence detector that simultaneously binds two signals to drive ER export. *Curr. Biol.* **25**, 403–412.
- Palade, G. E. (1975). Intracellular aspects of the process of protein synthesis. *Science* **189**, 347–358.
- Pfeffer, S. R. (2013). Rab GTPase regulation of membrane identity. *Curr. Opin. Cell Biol.* **25**, 414–419.
- Popoff, V., Adolf, F., Brugger, B. and Wieland, F. (2011). COPI budding within the Golgi stack. *Cold Spring Harb. Perspect. Biol.* **3**, a005231.
- Presley, J. F., Cole, N. B., Schroer, T. A., Hirschberg, C., Zaal, K. J. M. and Lippincott-Schwartz, J. (1997). ER-to-Golgi transport visualized in living cells. *Nature* **389**, 81–85.
- Sáenz, J. B., Sun, W. J., Chang, J. W., Li, J., Bursulaya, B., Gray, N. S. and Haslam, D. B. (2009). Golgicide A reveals essential roles for GBF1 in Golgi assembly and function. *Nat. Chem. Biol.* **5**, 157–165.
- Saito, K., Chen, M., Bard, F., Chen, S., Zhou, H., Woodley, D., Polischuk, R., Schekman, R. and Malhotra, V. (2009). TANGO1 facilitates cargo loading at endoplasmic reticulum exit sites. *Cell* **136**, 891–902.
- Saito, K., Yamashiro, K., Ichikawa, Y., Erlmann, P., Kontani, K., Malhotra, V. and Katada, T. (2011). cTAGE5 mediates collagen secretion through interaction with TANGO1 at endoplasmic reticulum exit sites. *Mol. Biol. Cell* **22**, 2301–2308.
- Salama, N. R., Yeung, T. and Schekman, R. W. (1993). The Sec13p complex and reconstitution of vesicle budding from the ER with purified cytosolic proteins. *EMBO J.* **12**, 4073–4082.
- Sanchez-Wandelmer, J., Ktistakis, N. T. and Reggiori, F. (2015). ERES: sites for autophagosome biogenesis and maturation? *J. Cell Sci.* **128**, 185–192.
- Scales, S. J., Pepperkok, R. and Kreis, T. E. (1997). Visualization of ER-to-Golgi transport in living cells reveals a sequential mode of action for COPII and COPI. *Cell* **90**, 1137–1148.
- Schimmoller, F., Singer-Kruger, B., Schroder, S., Kruger, U., Barlowe, C. and Riezman, H. (1995). The absence of Emp24p, a component of ER-derived COPII-coated vesicles, causes a defect in transport of selected proteins to the Golgi. *EMBO J.* **14**, 1329–1339.
- Schmiedeberg, L., Weisshart, K., Diekmann, S., Meyer Zu Hoerste, G. and Hemmerich, P. (2004). High- and low-mobility populations of HP1 in heterochromatin of mammalian cells. *Mol. Biol. Cell* **15**, 2819–2833.
- Snapp, E. L., Sharma, A., Lippincott-Schwartz, J. and Hegde, R. S. (2006). Monitoring chaperone engagement of substrates in the endoplasmic reticulum of live cells. *Proc. Natl. Acad. Sci. USA* **103**, 6536–6541.
- Soni, K. G., Mardones, G. A., Sougrat, R., Smirnova, E., Jackson, C. L. and Bonifacio, J. S. (2009). Coatomer-dependent protein delivery to lipid droplets. *J. Cell Sci.* **122**, 1834–1841.
- Tabak, H. F., Braakman, I. and van der Zand, A. (2013). Peroxisome formation and maintenance are dependent on the endoplasmic reticulum. *Annu. Rev. Biochem.* **82**, 723–744.
- Toomre, D., Keller, P., White, J., Olivo, J. C. and Simons, K. (1999). Dual-color visualization of trans-Golgi network to plasma membrane traffic along microtubules in living cells. *J. Cell Sci.* **112**, 21–33.
- Venditti, R., Scanu, T., Santoro, M., Di Tullio, G., Spaar, A., Gaibisso, R., Beznoussenko, G. V., Mironov, A. A., Mironov, A., Jr, Zelante, L. et al. (2012). Sedlin controls the ER export of procollagen by regulating the Sar1 cycle. *Science* **337**, 1668–1672.
- Venditti, R., Wilson, C. and De Matteis, M. A. (2014). Exiting the ER: what we know and what we don't. *Trends Cell Biol.* **24**, 9–18.
- Wacker, I., Kaether, C., Kromer, A., Migala, A., Almers, W. and Gerdes, H. H. (1997). Microtubule-dependent transport of secretory vesicles visualized in real time with a GFP-tagged secretory protein. *J. Cell Sci.* **110**, 1453–1463.
- Ward, T. H., Polishchuk, R. S., Caplan, S., Hirschberg, K. and Lippincott-Schwartz, J. (2001). Maintenance of Golgi structure and function depends on the integrity of ER export. *J. Cell Biol.* **155**, 557–570.
- Wendeler, M. W., Paccaud, J.-P. and Hauri, H.-P. (2007). Role of Sec24 isoforms in selective export of membrane proteins from the endoplasmic reticulum. *EMBO Rep.* **8**, 258–264.
- Witte, K., Schuh, A. L., Hegermann, J., Sarkeshik, A., Mayers, J. R., Schwarze, K., Yates, J. R., III, Eimer, S. and Audhya, A. (2011). TFG-1 function in protein secretion and oncogenesis. *Nat. Cell Biol.* **13**, 550–558.
- Yonekawa, S., Furuno, A., Baba, T., Fujiki, Y., Ogasawara, Y., Yamamoto, A., Tagaya, M. and Tani, K. (2011). Sec16B is involved in the endoplasmic reticulum export of the peroxisomal membrane biogenesis factor peroxin 16 (Pex16) in mammalian cells. *Proc. Natl. Acad. Sci. USA* **108**, 12746–12751.
- Zanetti, G., Pahuja, K. B., Studer, S., Shim, S. and Schekman, R. (2011). COPII and the regulation of protein sorting in mammals. *Nat. Cell Biol.* **14**, 20–28.
- Zoppino, F. C., Militello, R. D., Slavin, I., Álvarez, C. and Colombo, M. I. (2010). Autophagosome formation depends on the small GTPase Rab1 and functional ER exit sites. *Traffic* **11**, 1246–1261.